Available online at www.sciencedirect.com
ScienceDirect
Journal of Sound and Vibration 305 (2007) 34–49
JOURNAL OF SOUND AND VIBRATION
www.elsevier.com/locate/jsvi

Experimental characterization of multiple cracks in a cantilever beam utilizing transient vibration data following a probabilistic approach

H.F. Lam[a,*], C.T. Ng[a], M. Veidt[b]

[a]*Department of Building and Construction, City University of Hong Kong, 83 Tat Chee Avenue, Kowloon, Hong Kong*
[b]*School of Engineering, The University of Queensland, Brisbane, Queensland, Australia*

Received 1 December 2006; received in revised form 14 March 2007; accepted 17 March 2007

Abstract

This paper puts forward a practical method for detecting multiple cracks on beams by utilizing transient vibration data. To explicitly address the uncertainty that is induced by measurement noise and modeling error, the Bayesian statistical framework is followed in the proposed crack detection method, which consists of two stages. In the first stage the number of cracks is identified by a computationally efficient algorithm that utilizes the Bayesian model class selection method. In the second stage, the posterior probability density function (PDF) of crack characteristics (i.e., the crack locations and crack depths) are determined by the Bayesian model updating method. The feasibility of the proposed methodology is experimentally demonstrated using a cantilever beam with one and two artificial cracks with depths between 0% and 50% of the beam height. The experimental data consists of transient vibration time histories that are collected at a single location using a laser Doppler vibrometer measurement system and impact excitations at three locations along the beam. The results show that the two-stage procedure enables the identification of the correct number of cracks and corresponding locations and extents, together with the coefficient of variation (COV).

1. Introduction

The safety of structures, such as buildings and bridges, and their structural components, such as beams, columns, slabs, and canopies, are of serious public concern in all developed countries. Reliable and efficient structural damage detection methods are of primary importance in addressing such public concern.

Changes in dynamic characteristics have frequently been employed as a means of structural damage detection. A comprehensive review of recent developments can be found in Ref. [1]. Due to advances in sensor technologies, inspection devices such as laser Doppler vibrometers and shearographs have been developed to enable the measurement of accurate dynamic structural responses. However, the development of methodologies and algorithms to extract useful information from the measured data for structural damage

*Corresponding author. Tel.: +852 2788 7303; fax: +852 2788 7612.
E-mail address: paullam@cityu.edu.hk (H.F. Lam).

0022-460X/$ - see front matter © 2007 Elsevier Ltd. All rights reserved.
doi:10.1016/j.jsv.2007.03.028

detection is still immature. The goal of this paper is to make a seminal contribution in this area by developing a practical and reliable methodology for detecting cracks on structural members and verify it experimentally.

Many researchers have studied the use of dynamic measurement in crack detection on structural members. For detecting the existence of cracks and the corresponding locations, a non-model based approach, which relies on the measured responses of the undamaged (healthy) and possibly damaged structural member, is commonly used (e.g. Ref. [2]). However, a model-based approach, which involves modeling the structural members, has to be adopted if the crack extent (depth) is to be quantified.

To study the feasibility of the model-based approach, the majority of methods were focusing on single crack situations [3–8]. To extend the approach to a multi-crack situation, Ostachowicz and Krawczuk [9] studied the forward problem of a beam structure with two cracks in 1991. They expressed the changes in modal parameters as a function of crack locations and extents. In 1993, Hu and Liang [10] combined two different models to identify multiple cracks. One of the models involved the use of massless springs with infinitesimal lengths to represent the local flexibility introduced by a crack; and the other model incorporated the effective stress concept in continuum damage mechanics and Hamilton's principle. In 2005, Law and Lu [11] proposed to use measured time-domain responses in detecting multi-cracks on a beam structure through optimization algorithms. All of the abovementioned crack detection methods are only applicable in single-crack situations or when the number of cracks is known in advance, which is normally not possible in real situations.

The proposed crack detection methodology addresses this difficulty by dividing the process into two stages. The number of cracks is identified in the first stage, and the crack characteristics are identified in the second stage. The proposed methodology focuses on cases in which cracks are obstructed and therefore the vibration data at and near to the damaged region cannot be obtained. Furthermore, the proposed methodology is applicable even when the measurement of the undamaged (reference) structure is not available.

Due to the problem of "incomplete" measurement and measurement noise, the results of crack detection, such as the identified crack locations and depths, are uncertain. In the proposed methodology, these uncertainties are explicitly treated by the Bayesian statistical framework. Consequently, the proposed methodology not only calculates the crack locations and extents, but also the corresponding confidence level, providing engineers with valuable information to make informed judgments on remedial work.

For a crack detection method to be practical and efficient, it must be applicable with a small number of sensors. Otherwise, the equipment installation time and cost will seriously affect the applicability of the method. A particular advantage of the proposed methodology is that only one sensor is required, and the experimental verification result shows that enough information can be extracted from impacts at three locations along the structural member in the cases considered. It must be pointed out that the single sensor and multiple excitation technique is a practical measurement system for frame and truss structures in civil and mechanical applications (e.g., cranes and draglines) [2].

This paper consists of two main parts: the theoretical development of the methodology and the experimental case studies. In the first part (Section 2), the analytical beam model, the method for detecting the number of cracks (stage one of the proposed methodology), and the method for identifying the crack characteristics (stage two) are described. The second part (Section 3) presents the results of a series of comprehensive experimental case studies in demonstrating the proposed crack detection methodology. Conclusions are drawn in Section 4.

2. Methodology and background theories

In the first sub-section, details of the modeling of the cracked beam with semi-rigid connection and its parameterization are addressed. In the second sub-section, the main problem of identifying the number of cracks following a model-based approach is discussed. That is followed by the first stage of the proposed crack detection methodology, namely the determination of the number of cracks, which relies on a computationally efficient algorithm and the Bayesian model class selection method. In the last sub-section, the second stage of the proposed methodology, which aims in identifying the crack locations and extents following the Bayesian model updating method, is briefly reviewed.

2.1. Modeling of semi-rigidly connected cantilever beam with multiple cracks

Fig. 1 shows a model of a cantilever beam with N_C cracks. The beam is divided into N_C+1 segments, each with length l_i, for $i = 1, \ldots, N_C+1$, where $\sum_{i=1}^{N_C+1} l_i = L$. Each segment is modeled as an Euler–Bernoulli beam with the equation of motion for vibration under an arbitrary force $P(t)$ as

$$EI\frac{\partial^4 y(x,t)}{\partial x^4} + \bar{m}\frac{\partial^2 y(x,t)}{\partial t^2} = P(t), \tag{1}$$

where EI is the flexural rigidity, $\bar{m}$ is the mass per unit length, and y is the transverse deflection of the beam, which is a function of the position x along the beam and time t. By using separation of variables $y(x, t) = \phi(x)z(t)$, the displacement $y(x, t)$ is described as the product of the modal function $z(t)$ and the mode shape function $\phi(x)$. The general solution of the mode shape functions $\phi_i(x_i)$ for the ith segment can be expressed as

$$\phi_i(x_i) = C_i\sin(\beta x_i) + D_i\sinh(\beta x_i) + E_i\cos(\beta x_i) + F_i\cosh(\beta x_i) \text{ for } i = 1, \ldots, N_C+1, \tag{2}$$

where $\beta^4 = \omega^2\bar{m}/EI$; ω is the angular natural frequency of the system in radians per second, and C_i, D_i, E_i, and F_i are unknown coefficients to be calculated from the boundary and continuity conditions. The boundary conditions at the fixed and free ends, respectively, are:

$$\begin{aligned} \phi_1(0) &= 0, \\ K\frac{d\phi_1(0)}{dx} &= EI\frac{d^2\phi_1(0)}{dx^2}, \\ \frac{d^2\phi_{N_C+1}(l_{N_C+1})}{dx^2} &= 0, \\ \frac{d^3\phi_{N_C+1}(l_{N_C+1})}{dx^3} &= 0, \end{aligned} \tag{3}$$

where K is the stiffness coefficient of the rotational spring at the left end of the cantilever beam. The rotational spring models the semi-rigid behavior of the beam end connection [12]. At the general ith crack of the beam, the following four continuity conditions must be satisfied:

$$\begin{aligned} \phi_i(l_i) &= \phi_{i+1}(0), \\ \frac{d\phi_{i+1}(0)}{dx} - \frac{d\phi_i(l_i)}{dx} &= \Delta_i L\frac{d^2\phi_{i+1}(0)}{dx^2}, \\ \frac{d^2\phi_i(l_i)}{dx^2} &= \frac{d^2\phi_{i+1}(0)}{dx^2}, \qquad \text{for } i = 1, \ldots, N_C \\ \frac{d^3\phi_i(l_i)}{dx^3} &= \frac{d^3\phi_{i+1}(0)}{dx^3}, \end{aligned} \tag{4}$$

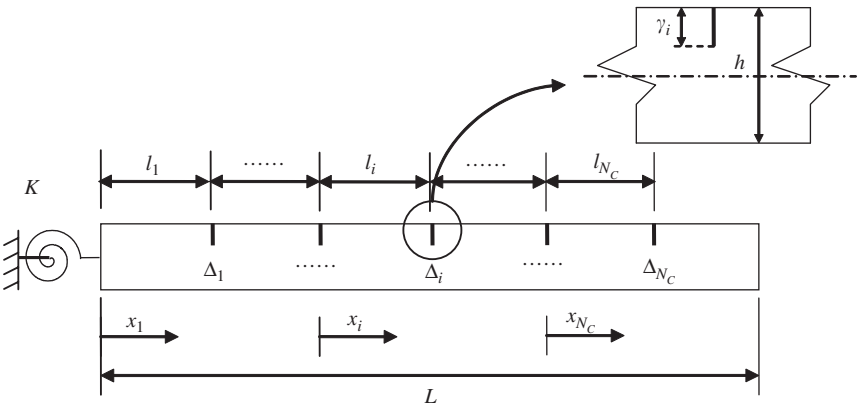

Fig. 1. The model of a cracked cantilever beam with semi-rigid connection.

where Δ_i is the non-dimensional flexibility parameter to characterize the extent of the ith crack. The relationship between the crack extent Δ_i and the crack depth ratio $\delta_i = \gamma_i/h$ can be found in Ref. [9] as

$$\Delta_i = 6\pi\delta_i^2\left(\frac{h}{L}\right)f(\delta_i), \tag{5}$$

where h is the beam depth, γ_i is the depth of the ith crack, and the function $f(\delta_i)$ is given by [9]

$$f(\delta_i) = 0.6384 - 1.035\delta_i + 3.7201\delta_i^2 - 5.1773\delta_i^3 + 7.553\delta_i^4 - 7.332\delta_i^5 + 2.4909\delta_i^6. \tag{6}$$

A characteristic equation of the cracked beam can be obtained by substituting the conditions in Eqs. (3) and (4) into Eq. (2). An infinite number of natural frequencies ω_k and mode shapes $\phi_k(x)$ for $k = 1,\ldots, \infty$ of the system can then be calculated. In the under-damped vibration case, the modal function of the kth mode $z_k(t)$ is in the following form:

$$z_k(t) = e^{-\zeta_k\omega_k t}\left(A_k \sin\omega_{D,k}t + B_k\cos\omega_{D,k}t\right), \tag{7}$$

where A_k and B_k depend on the initial conditions of the kth system and $\omega_{D,k} = \omega_k\sqrt{1-\zeta_k^2}$ and ζ_k are the damped frequency and the critical damping ratio of the kth mode. The overall response of the beam can be calculated by the method of modal superposition [13]. In general, only a small number of lower modes contribute to the dynamic response of the system, and this number depends on many factors, such as the support conditions and the types of excitations.

According to Katafygiotis et al. [14], the uncertainty that is associated with the stiffness K of the rotational spring, which is employed to model the semi-rigid connection, is much larger than those associated with other model parameters, such as the modulus of elasticity and the mass density of the structural member. Therefore, the rotational stiffness will be included as one of the uncertain parameters in the proposed methodology. To prevent numerical problems, a normalized rotational stiffness $\tilde{K} = K/EI$ is used. Furthermore, damping is usually more difficult to identify when compared to other model parameters. Thus, the damping ratios are also included as uncertain parameters in the proposed methodology. It must be pointed out that increasing the number of uncertain parameters by including these system characteristics will increase the uncertainties associated with the identified damage parameter results, i.e. crack locations and extents. The effects of including these additional uncertain parameters in the proposed methodology have been comprehensively studied in Ref. [15] and will not be repeated in this paper.

In the proposed methodology, the uncertain parameter vector for a beam with j cracks is

$$\mathbf{a}_j = \left\{\tilde{K}, \zeta_1, \ldots\zeta_q, l_1, l_2, \ldots l_j, \Delta_1, \Delta_2, \ldots, \Delta_j\right\}^{\mathrm{T}}, \tag{8}$$

where q is the number of modes required to describe with sufficient accuracy the dynamic response of the cantilever beam for a particular excitation. In the experimental case study, the first four modes are used. The total number of uncertain parameters is $2j+q+1$.

2.2. Identification of the number of cracks (stage one)

If the model-based approach is followed for crack detection and the number of cracks is not known, beams with different numbers of cracks have to be modeled by different classes of models, as shown in Fig. 2. In the figure, the model class M_j is employed in modeling a beam with j cracks, and the parameters l_j and Δ_j are used to describe the location and extent of the jth crack.

The problem is how to identify the "optimal" model class using a set of measurements D. By following the concept of model updating, one may consider carrying out a minimization for each model class to minimize the discrepancy between the measured and modeled responses, and "pick up" the "optimal" model class as that which can give the best fit to the measurement. It must be pointed out that the selection of the "optimal" model class based on a given set of data is not trivial. It is clear that the model class of a beam with more cracks consists of more model parameters (see Fig. 2), which will always provide a better fit to the measurement when compared to a model class with fewer parameters. Hence, the selection of model class

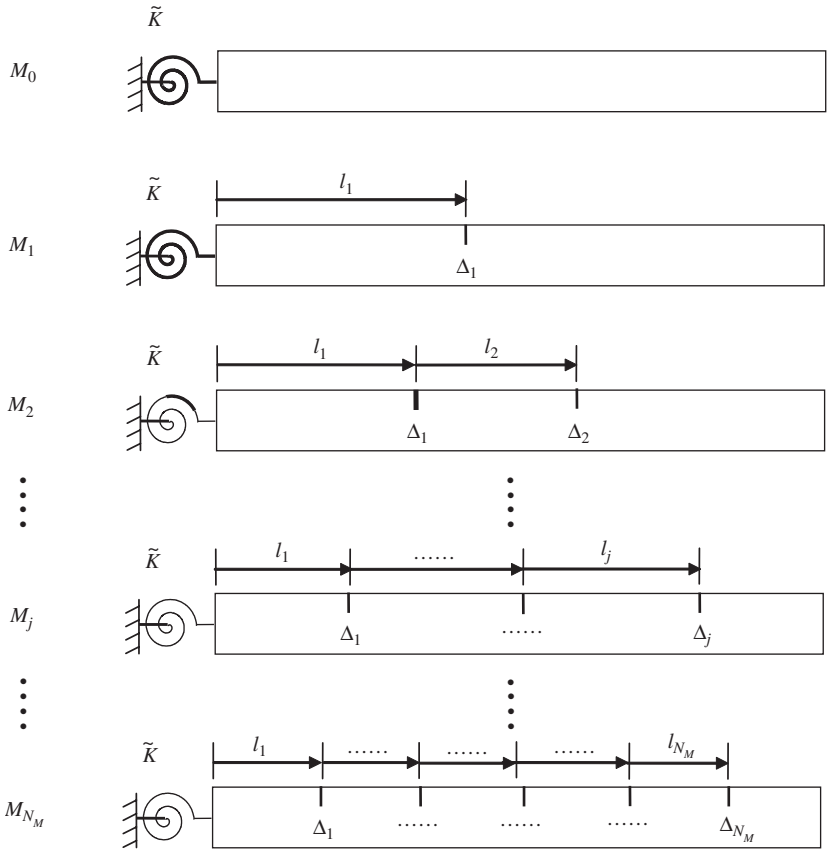

Fig. 2. Schematic diagram illustrating the basic strategy for the first stage of the proposed methodology.

based solely on the fitting between the modeled and the measured dynamic responses can be very misleading, as the most complex model class will always be selected.

In addressing this problem, the first stage of the proposed methodology relies on the Bayesian model class selection method [16] in selecting the "optimal" model class to identify the number of cracks on the beam. Due to space limitations here, the Bayesian model class selection method will only be briefly reviewed. Interested readers should consult Ref. [16]. The original goal of the method is to select the "optimal" class of models from a given list of N_M model classes. The selection is based on the probability of the model class conditional on the set of measurements D [16]:

$$P(M_j|D,U) = \frac{p(D|M_j,U)P(M_j|U)}{p(D|U)} \quad \text{for } j = 1,\ldots,N_M, \tag{9}$$

where U expresses the user's judgment about the initial plausibility of the classes of models, expressed as a prior probability $p(M_j|U)$ on the model class M_j, such that $\sum_{j=1}^{N_M} P(M_j|U) = 1$. Unless there is prior information about the number of cracks on the beam, the prior probability $p(M_j|U)$ is taken as $1/N_M$; $1/p(D|U)$ is treated as a normalizing constant. The most important term in Eq. (9) is $p(D|M_j, U)$, which is known as the "evidence" for the model class M_j provided by the data D. The class of models to be used is obviously the one that maximizes the probability $P(M_j|D, U)$ and this is generally equivalent to the one that maximizes the evidence $p(D|M_j, U)$ with respect to M_j. In the application of the Bayesian model class selection method in the detection of the number of cracks, subjective judgment from engineers is not preferred. As a result, U is dropped in $p(D|M_j\ U)$ because it is assumed that M_j alone specifies the probability density function (PDF) for the data. Hence, the evidence $p(D|M_j, U) = p(D|M_j)$ hereafter.

For a globally identifiable case [17,18], the evidence can be calculated based on an asymptotic approximation [19]:

$$p(D|M_j) \approx p\,(D|\hat{\mathbf{a}}_j, M_j)(2\pi)^{N_j/2} p\,(\hat{\mathbf{a}}_j|M_j)\left|\mathbf{H}_j(\hat{\mathbf{a}}_j)\right|^{-1/2}, \quad \text{for } j = 1,\ldots,N_M, \tag{10}$$

where $\hat{\mathbf{a}}_j$ denotes the optimal model in the model class M_j (the set of optimal model parameters of $\mathbf{a}_j$). N_j is the number of uncertain model parameters in $\hat{\mathbf{a}}_j$, and $\mathbf{H}_j(\hat{\mathbf{a}}_j)$ is the Hessian of the function $g(\mathbf{a}_j) = -\ln\left[p(\mathbf{a}_j|M_j)p(D|\mathbf{a}_j, M_j)\right]$ evaluated at the optimal model $\hat{\mathbf{a}}_j$.

The evidence $p(D|M_j)$ in Eq. (10) consists of two factors. The first factor $p(D|\hat{\mathbf{a}}_j, M_j)$ is the likelihood factor. This will be larger for those model classes that give a better "fit" to the data D. This favors model classes with more parameters (model classes with higher complexity). The second factor $(2\pi)^{N_j/2}p(\hat{\mathbf{a}}_j|M_j)|\mathbf{H}_j(\hat{\mathbf{a}}_j)|^{-1/2}$ is called the Ockham factor [20]. Beck and Yuen [16] showed that the value of the Ockham factor decreases as the number of uncertain parameters in the model class increases and therefore provides a mathematically rigorous and robust penalty against parameterization. The combination of these two factors enables the selection of the "simplest" model class that can provide a "good fit" to the measurement.

With the help of the Bayesian model class selection method, the computationally efficient algorithm is developed for identifying the number of cracks on the beam utilizing the given set of measurement D. The algorithm consists of a series of iteration steps, as shown in Fig. 3, and begins by testing the simplest class of models with no crack on the beam. Value zero is assigned to the variable j, which is the number of cracks at the current iteration step. In a general iteration step, the algorithm compares the model class that has j cracks with the one that has $j+1$ cracks following the Bayesian model class selection method. If the evidence of the model class with j cracks is larger than that of the model class with $j+1$ cracks, then the algorithm stops and the number of cracks is equal to j. Otherwise, the algorithm will assign $j = j+1$ and repeat the comparison (see Fig. 3).

2.3. Identification of crack locations and depths (stage two)

After identifying the number of cracks, for example N_C by the proposed algorithm in stage one, the goal in the second stage is to calculate the posterior PDF $p\left(\mathbf{a}_{N_C}|D, M_{N_C}\right)$ of the set of uncertain model parameters $\mathbf{a}_{N_C}$

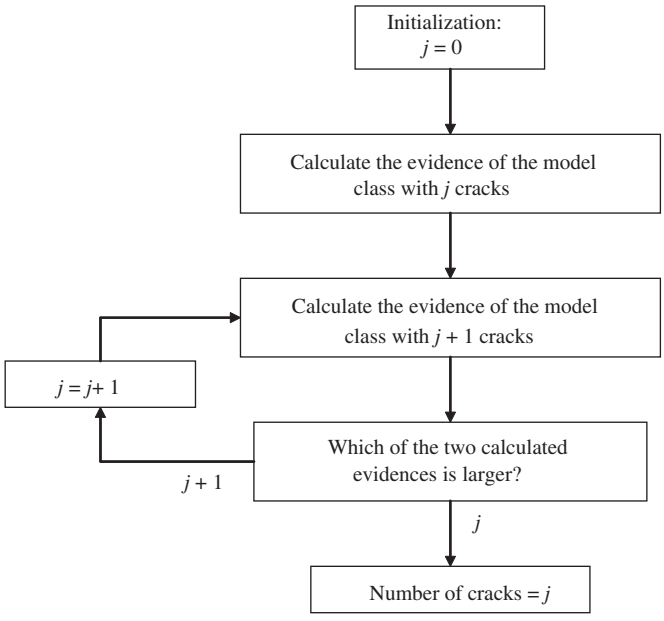

Fig. 3. The proposed algorithm for identifying the number of cracks in the first stage of the proposed methodology.

in the model class M_{N_C}. For identifiable cases, the posterior PDF of uncertain model parameters conditional on the measurement D and the model class M_{N_C} can be approximated as [17,18]:

$$p(\mathbf{a}_{N_C}|D, M_{N_C}) \approx \sum_{\alpha=1}^{N_\alpha} w_\alpha \mathbf{N}\left(\hat{\mathbf{a}}_{N_C}^{(\alpha)}, A_N^{-1}(\hat{\mathbf{a}}_{N_C}^{(\alpha)})\right), \tag{11}$$

where $\hat{\mathbf{a}}_{N_C}^{(\alpha)}$ for $\alpha = 1,\ldots,N_\alpha$ are the output-equivalent optimal models of the system, which can be obtained using the algorithm presented in Ref. [18]; $\mathbf{N}(\boldsymbol{\mu}, \boldsymbol{\Sigma})$ denotes a multivariate Gaussian distribution with mean $\boldsymbol{\mu}$ and covariance matrix $\boldsymbol{\Sigma}$. The matrix $A_N\left(\hat{\mathbf{a}}_{N_c}^{(\alpha)}\right)$ is the Hessian of the function $N_J \ln J(\mathbf{a}_{N_C}|D, M_{N_C})$ evaluated at $\hat{\mathbf{a}}_{N_C}^{(\alpha)}$, where $N_J = (NN_o - 1)/2$, and $J(\mathbf{a}_{N_C}|D, M_{N_C})$ is given by

$$J(\mathbf{a}_{N_C}|D, M_{N_C}) = \frac{1}{NN_O}\sum_{k=1}^{N} \left\|\Psi(k; \mathbf{a}_{N_C}, M_{N_C}) - \hat{\Psi}(k)\right\|^2. \tag{12}$$

The weighting coefficients in Eq. (11) are given by

$$w_\alpha = \frac{w'_\alpha}{\sum_{\alpha=1}^{N_\alpha} w'_\alpha}, \quad \text{where } w'_\alpha = \pi\left(\hat{\mathbf{a}}_{N_C}^{(\alpha)}\right)\left|A_N\left(\hat{\mathbf{a}}_{N_C}^{(\alpha)}\right)\right|^{-1/2}, \tag{13}$$

where N is the total number of measured data points of the observed degree of freedom (DOF); N_O is the number of observed DOFs; $\hat{\psi}(k)$ is the vector of measured response; $\hat{\psi}(k; \mathbf{a}_{N_C}, M_{N_C})$ is the vector of calculated response (at the observed DOFs) at the kth time step for the optimal models $\mathbf{a}_{N_C}$ in M_{N_C}; $\pi\left(\hat{\mathbf{a}}_{N_C}^{(\alpha)}\right)$ is the prior PDF of the set of uncertain model parameters $\mathbf{a}_{N_C}$ evaluated at $\hat{\mathbf{a}}_{N_C}^{(\alpha)}$, which allows engineering judgment to be incorporated in the analysis.

Instead of pinpointing the crack locations and extents as in the deterministic approach, the proposed crack detection methodology focuses on calculating the posterior PDF of the model parameters $\mathbf{a}_{N_C}$. As a result, the confidence level of the crack detection results can be quantified through the calculated probability or the corresponding coefficient of variation (COV). This information is extremely important for engineers who are making judgments about remedial work.

3. Experimental verification

The proposed crack detection methodology was demonstrated and verified using the cantilever beam test system as shown in Fig. 4. The test sample is an aluminum bar with Young's modulus $E = 69$ GPa, density $\rho = 2960\,\text{kg/m}^3$, width $b = 12$ mm, height $h = 6$ mm and the length of the aluminum bar is 600 mm. The first 200 mm of the beam is fixed in a rigid clamping system, and the length of the cantilever beam is therefore 400 mm. Fig. 5 shows the excitation locations, measurement location and crack locations on the cantilever. The cantilever beam is excited at three points ($e_1 = 50 \pm 1$ mm, $e_2 = 200 \pm 1$ mm and $e_3 = 300 \pm 1$ mm from the fixed end) using a 086D80 PCB Piezotronics impact hammer with a 5 mm thick steel backing mass and a nylon tip together with a 480C02 ICP sensor signal conditioner. The transient transverse vibration response is measured at 220 ± 1 mm from the fixed end using a Polytec laser vibrometer system with an OFV-502 fiber-optic laser head and an OVD-02 velocity demodulator set at 125 mm/s/V measurement resolution.

The response signal is collected for 500 ms with an approximately 50 ms pre-trigger with a temporal resolution of 0.2 ms. Fig. 6 shows typical time histories measured at the sensor for the three excitation locations. The three graphs highlight the different characteristics of the response signals depending on the impact location.

Artificial cracks c_1 and c_2 are machined into the beam using a bandsaw with a blade thickness of approximately 1 mm. The locations of the cracks are $l_1 = 80 \pm 1$ mm and $l_2 = 100 \pm 1$ mm (see Fig. 5) as measured from l_1. Experimental data were collected for three depths of the second crack. The nominal crack depths are 2.8 mm for c_1 and 0.8, 1.7, and 3.2 mm for c_2 with an estimated uncertainty of ± 0.15 mm. Fig. 7 shows the response signals in time and frequency space for excitation at position e_2 for the cases of the

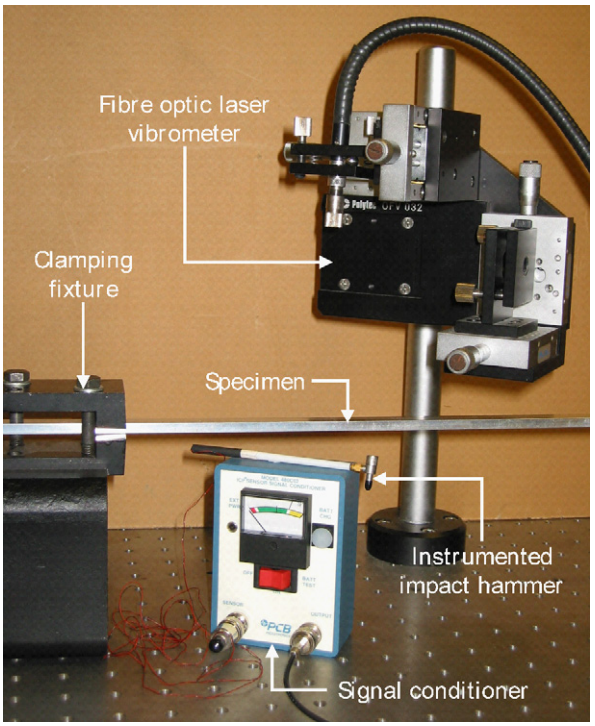

Fig. 4. Cantilever beam experiment configuration.

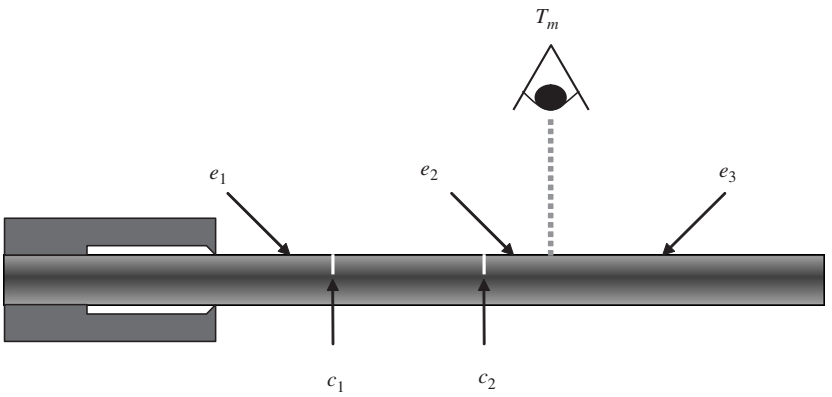

Fig. 5. Excitation location e_u ($u = 1$, 2, and 3), measurement location T_m, and crack locations $c =$ ($i = 1$, 2).

uncracked beam and the beam with cracks c_1 and c_2 extended to their maximum depths, i.e. $\gamma_1 = 2.8 \pm 0.15$ and $\gamma_2 = 3.2 \pm 0.15$ mm respectively. It should be noted that the response signal in time space is normalized so that the maximum amplitude is equal to unity for the uncracked and cracked beams. The signals confirm that, as expected, the natural frequencies for the cracked beam are shifted to lower frequencies, but they also show that these frequency shifts are small, especially for the first two vibration modes and considering that the data of the cracked beam is for the maximum crack depths of both cracks c_1 and c_2. Hence, damage detection using modal parameter identification techniques, e.g. Ref. [21], will be difficult.

The calibration constant of the instrumented impact hammer is given as 17 mV/N. This parameter had to be adjusted, since a steel backing mass was used to increase the excitation strength, especially for the higher vibration modes. In addition, as always in impact testing using a handheld hammer, there was a slight variation in the direction of impact relative to the axis of the beam from experiment to experiment.

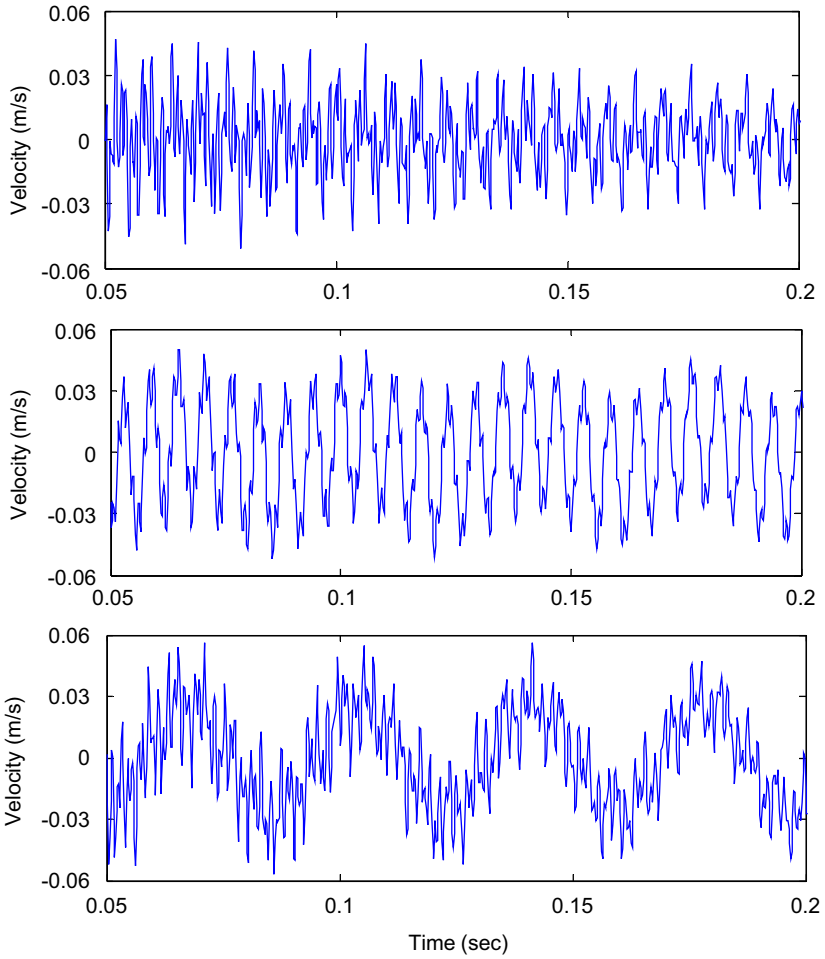

Fig. 6. Impact response signals for the three excitation locations (Top: e_1, middle: e_2, bottom: e_3).

Table 1
Summary of all cases in the experimental study

Case	N_C	Crack location (mm)	Crack extent	Crack depth (mm)
A	0	N/A	N/A	N/A
B	1	$l_1 = 80 \pm 1$	$\Delta_1 = 0.0407$	2.8 ± 0.15
C	2	$l_1 = 80 \pm 1$, $l_2 = 100 \pm 1$	$\Delta_1 = 0.0407$ $\Delta_2 = 0.0028$	2.8 ± 0.15 0.8 ± 0.15
D	2	$l_1 = 80 \pm 1$, $l_2 = 100 \pm 1$	$\Delta_1 = 0.0407$ $\Delta_2 = 0.0128$	2.8 ± 0.15 1.7 ± 0.15
E	2	$l_1 = 80 \pm 1$, $l_2 = 100 \pm 1$	$\Delta_1 = 0.0407$ $\Delta_2 = 0.0572$	2.8 ± 0.15 3.2 ± 0.15

Consequently, the effective excitation force perpendicular to the beam was calculated by matching the signal amplitudes of the first few cycles of the simulated and measured response signals. Considering these two effects, the effective calibration constants for the excitation forces used in the simulation varied between 30.9 and 40.7 mV/N.

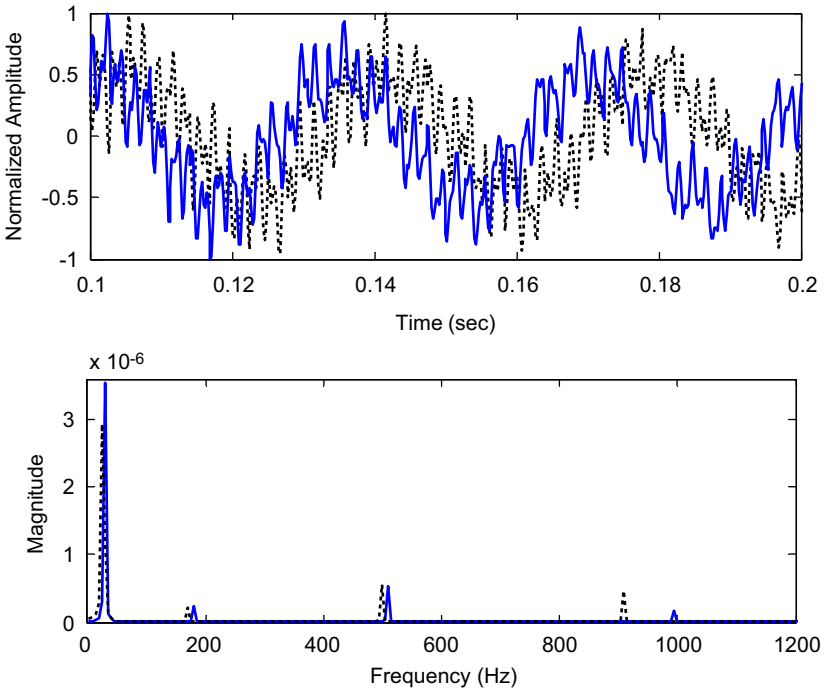

Fig. 7. Impact response signals in time and frequency domain for the uncracked (solid) and cracked (dashed) beam (excitation position at e_2, cracks c_1 and c_2 are in full depths).

Table 2
Vector of uncertain parameters of the identification model in each case

Case	Uncertain parameters of the identification model
A	$\mathbf{a}_0 = \{\tilde{K}, \zeta_1, \zeta_2, \zeta_3, \zeta_4\}^{\mathrm{T}}$
B	$\mathbf{a}_1 = \{\tilde{K}, \zeta_1, \zeta_2, \zeta_3, \zeta_4, l_1, \Delta_1\}^{\mathrm{T}}$
C, D, and E	$\mathbf{a}_2 = \{\tilde{K}, \zeta_1, \zeta_2, \zeta_3, \zeta_4, l_1, \Delta_1, l_2, \Delta_2\}^{\mathrm{T}}$

Table 1 gives a list of the particular experimental configurations analyzed for this paper. Case A is the beam without cracks. Case B has crack c_1 at location $l_1 = 80 \pm 1$ mm from the semi-rigid end with depth $\gamma_1 = 2.8 \pm 0.15$ mm (i.e. the nominal value $\delta_1 = 0.4667$ and $\Delta_1 = 0.0407$). The robustness and sensitivity of the proposed methodology is investigated in Cases C, D, and E with two cracks, c_1 at $l_1 = 80 \pm 1$ mm and c_2 at $l_2 = 100 \pm 1$ mm measured from c_1. In all three cases, c_1 has a depth of $\gamma_1 = 2.8 \pm 0.15$ mm whereas the depth of the second crack c_2 varies from a shallow crack to an approximately half-thickness crack. The nominal values of the crack parameters for crack c_2 are $\gamma_2 = [0.8\,\text{mm}, 1.7\,\text{mm}, 3.2\,\text{mm}]$, $\delta_2 = [0.1333, 0.2833, 0.5333]$, and $\Delta_2 = [0.0028, 0.0128, 0.0572]$, respectively.

As shown in Fig. 7, it is clear from the spectrum that only the first four modes significantly contribute to the measured responses. Hence, only the first four modes are considered in the dynamic analysis. Furthermore, the system is assumed to be classically damped with different critical damping ratios for different modes. The uncertain parameter vector for different cases can then be obtained using Eq. (8), and the identification models that are adopted in different cases are summarized in Table 2.

Table 3
The results of Bayesian model class selection in all cases

Case	Class of models	Logarithm of the evidence	Logarithm of the likelihood factor	Logarithm of the Ockham factor
A	M_0	**25095**	25117	−22
	M_1	25091	25122	−31
B	M_0	21525	21532	−7
	M_1	**31789**	31828	−39
	M_2	31778	31830	−52
C	M_0	16706	16710	−4
	M_1	25000	25040	−40
	M_2	**27668**	27728	−60
	M_3	27658	27729	−71
D	M_0	15776	15788	−12
	M_1	21628	21656	−28
	M_2	**28914**	28974	−60
	M_3	28906	28975	−69
E	M_0	15243	15248	−5
	M_1	23020	23058	−38
	M_2	**31018**	31083	−65
	M_3	30993	31084	−91

3.1. Identified number of cracks (stage one)

Table 3 shows the results of the first stage of the proposed crack detection methodology for all five cases. The larger the value of the evidence, the higher the probability of the model class conditional on the data D. The logarithm is used because the numerical values of the evidence are usually very large, which may cause computational problems. The number of cracks can then be identified based on the value of the logarithm of the evidence. From Table 3, it is clear that M_0 (no crack) and M_1 (single crack) are selected for Case A and Case B, respectively, while M_2 is selected for Cases C, D, and E. The proposed methodology successfully identifies the true number of cracks in all cases.

Table 3 also shows the likelihood and Ockham factors of the evidence for all cases. The logarithm of the likelihood factor, which shows the ability of the model class in fitting the measurement, will increase when the complexity of the model class increases (beams with more cracks). Hence, it is not possible to only use the likelihood factor in selecting the "optimal" model class to identify the number of cracks. The value of the logarithm of the Ockham factor for all cases will be smaller (i.e., the logarithm will become more negative) when the complexity of the model class increases. Hence, the Ockham factor penalizes the complexity of the model class in the evidence.

This is a very important result because it has been achieved without any subjective judgment from the user and any prior knowledge (i.e., a prior probability $P(M_j|U)$ in Eq. (9)). Hence, the decision of how many cracks to include in the damage characterization process relies purely on the set of measurement D.

3.2. Identified crack characteristics (stage two)

In the second stage of the proposed methodology, the set of "optimal" parameters is identified and the PDF of the uncertain parameters, which consists of the crack parameters and the beam properties, is approximated by Eq. (11). Table 4 summarizes the identified "optimal" crack parameters, and the normalized marginal PDF of the crack parameters in Case B is shown in Fig. 8. As there is only one optimal model within the domain of interest, there is only one peak in Fig. 8. The figure also shows that the PDF value drops significantly when one moves away from the optimal model $\hat{\mathbf{a}}_1$. This is the typical characteristic of an identifiable case [14,22,23]. The marginal cumulative distributions of the crack parameters are plotted in Figs. 9 and 10. It is clear from the

Table 4
The results of crack evaluation in Cases B, C, D, and E

Case	Location(s) (mm)		Extent(s)		
	l_i (COV %)	True location	Δ_i (COV %)	Crack depth (mm)	True crack depth (mm)
B	$l_1 = 79.6$ (0.03)	80 ± 1	$\Delta_1 = 0.0451$ (0.12)	2.92	2.8 ± 0.15
C	$l_1 = 82.2$ (0.21)	80 ± 1	$\Delta_1 = 0.0492$ (0.34)	3.02	2.8 ± 0.15
	$l_2 = 102.6$ (1.15)	100 ± 1	$\Delta_2 = 0.0091$ (5.48)	1.44	0.8 ± 0.15
D	$l_1 = 82.4$ (0.24)	80 ± 1	$\Delta_1 = 0.0489$ (0.40)	3.01	2.8 ± 0.15
	$l_2 = 102.1$ (0.69)	100 ± 1	$\Delta_2 = 0.0171$ (3.47)	1.94	1.7 ± 0.15
E	$l_1 = 79.2$ (0.25)	80 ± 1	$\Delta_1 = 0.0479$ (0.30)	2.99	2.8 ± 0.15
	$l_2 = 106.4$ (0.20)	100 ± 1	$\Delta_2 = 0.0700$ (0.97)	3.46	3.2 ± 0.15

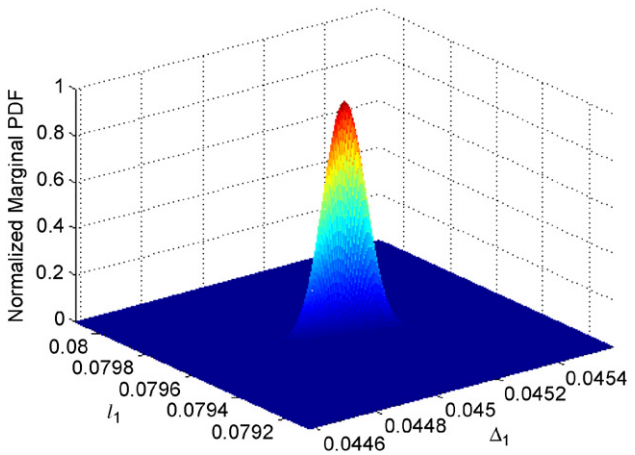

Fig. 8. Normalized marginal PDF of the crack location (l_1) and extent (Δ_1) in Case B.

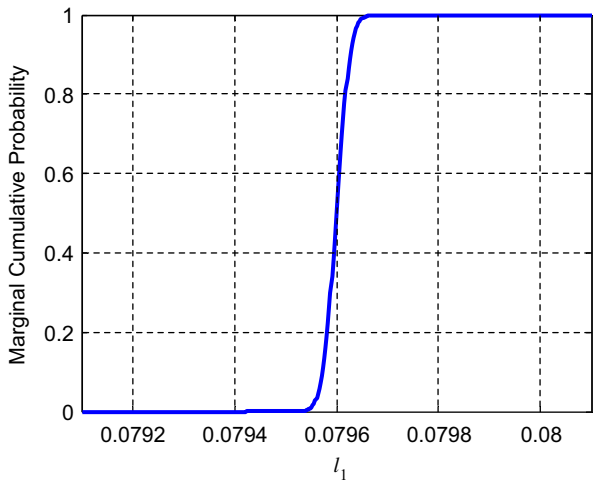

Fig. 9. Marginal cumulative distribution of the crack location (l_1) in Case B.

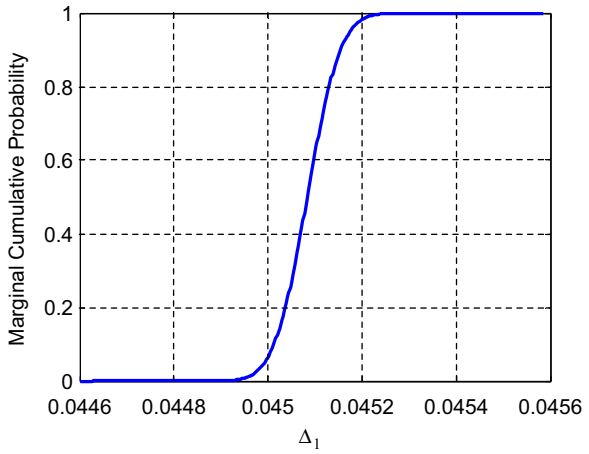

Fig. 10. Marginal cumulative distribution of the crack extent (Δ_1) in Case B.

figures that the uncertainties that are associated with the identified crack detection results are very low. In other words, the identified results are of high degree of confidence. To make the discussion on the uncertainty of the identification results more convenient, the coefficients of variation (COVs) of all uncertain parameters are calculated and summarized in Table 4.

The identified crack location and crack depth (79.6 and 2.92 mm) in the single crack case (Case B) in Table 4 are perfectly matched with the true values (80 ± 1 mm and 2.8 ± 0.15 mm). Furthermore, the COVs of the identified crack location and depth are very small, and the confidence level of the result of crack detection is therefore high. It can be concluded that the proposed crack detection methodology successfully identifies the crack location and depth in Case B.

There are two cracks in Case C: the first crack c_1 at 80 ± 1 mm is the same as that in Case B, and the second crack c_2 at 100 ± 1 mm is very small (0.8 ± 0.15 mm) at only about 13% of the overall depth of the beam. Hence, this case can be used to test the performance of the proposed methodology in detecting small cracks. The identified crack locations for both c_1 and c_2 in Case C in Table 4 are very close to the true values. As the COV value of the first crack location is smaller than that of the second crack location, the result shows that the second crack location is relatively more uncertain when compared to the first. This can be explained by the fact that the crack depth of the second crack is much smaller than that of the first crack (i.e., the first crack is more outstanding than the second). When the identified crack depths are considered, the identified crack depth of the first crack c_1 (3.02 mm) is closer to the true value (2.8 ± 0.15 mm) when compared to that of the second crack c_2. The relatively poor result for the second crack can be explained by the high uncertainty, which is clearly shown by the relatively large COV value of the identified crack depth of c_2. This case shows the importance of estimating the uncertainties associated with the identification results.

In Case D, the crack depth of c_2 is increased from 0.8 ± 0.15 mm to 1.7 ± 0.15 mm, which is about 28% of the overall depth of the beam. The identified crack locations in Case D are very similar to those in Case C except the COV value of the second crack location is relatively smaller when compared to that in Case C. This result is expected as the crack depth of c_2 is larger in Case D than in Case C. The identified crack depth of c_1 is very similar to that in Case C, and the identified crack depth of c_1 is much more accurate than that in Case C. This result aligns with the relatively small COV value in Δ_2 of Case D when compared to that of Case C.

In Case E, the crack depth of c_2 is further increased from 1.7 ± 0.15 mm to 3.2 ± 0.15 mm. Considering Case E in Table 4, the identified crack location and depth of c_1 are very similar as those in the previous cases. However, the identified crack location of c_2 is the worst among all cases. This result is unexpected as the crack depth of c_2 in Case E is the largest among all cases, and this crack should be the most outstanding. After carefully inspecting the second crack c_2 on the aluminum bar, the inaccuracy in the identified crack location of c_2 in Case E may be caused by the poor workmanship in increasing the crack depth of c_2 from Case D to Case E. Fig. 11 shows the crack c_2 in Case E. It is clear from the figure that the crack is not straight and the

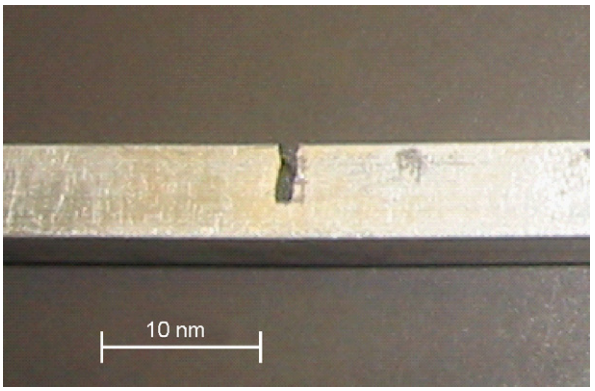

Fig. 11. The second crack c_2 in Case E.

Table 5
The results of beam property identification in all cases

Case	$\tilde{K}$ (COV %)	Damping Ratio (%) of each mode (COV %)			
		ζ_1	ζ_2	ζ_3	ζ_4
A	378.42 (0.10)	0% (—)	0.0021% (56.70)	0.3417% (3.31)	0.2001% (2.39)
B	428.64 (0.05)	0.0383% (16.84)	0.0123% (4.18)	0.0632% (1.72)	0.5367% (1.51)
C	740.48 (4.90)	0% (—)	0.0076% (11.08)	0.0876% (2.52)	0.0795% (1.25)
D	704.18 (5.43)	0% (—)	0.0085% (8.43)	0.0775% (2.33)	0.0731% (1.09)
E	403.65 (3.00)	0% (—)	0.0200% (3.92)	0.0761% (1.82)	0.0927% (0.96)

crack width is large; as a result, the modeling error becomes large. Even under such non-favorable conditions, the identified crack characteristics are still of acceptable accuracy.

3.3. Identified beam property parameters

Apart from the crack characteristics, several beam properties have to be included in the uncertain parameter vector $\mathbf{a}_j$. These include the normalized stiffness $\tilde{K}$ for modeling the semi-rigid connection of the cantilever beam and the damping ratios of the first four vibration modes. The inclusion of $\tilde{K}$ as uncertain parameter is essential in this study as the clamping condition changes every time the crack state in the beam is altered from case to case by bandsaw machining. In addition, the different thicknesses of the remaining material ligaments and the local characteristics at the groove of the artificial notch will influence the damping characteristics for every configuration and for every vibration mode. Hence, it is necessary to include the damping characteristics as uncertain parameters.

Table 5 shows the calculated beam properties for the five cases. The normalized rotational spring stiffness varies between 378 and 704. This confirms the well-known fact that it is extremely difficult to experimentally

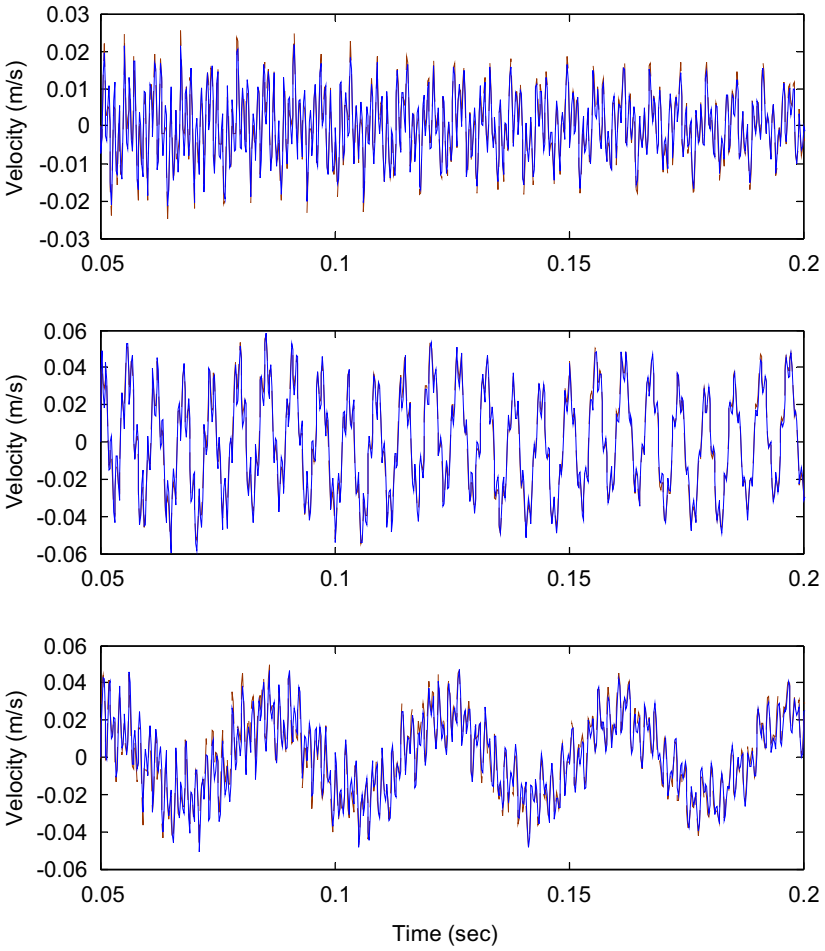

Fig. 12. Comparison of the simulated and measured time histories for Case B (Dash: measured, Solid: simulated) (Top: e_1, middle: e_2, bottom: e_3).

realize a fixed-end condition and to use a semi-rigid end condition in the analytical model is absolutely essential in the case of a "fixed" end.

For the relatively short observation period of 450 ms the fundamental mode turns out to be effectively undamped apart from Case B, which shows a small damping value ($\zeta_1 = 0.0383\%$) with large uncertainty (COV = 16.84%). Mode 2 shows also very little damping and the uncertainties in the calculated values are relatively large. Modes 3 and 4 show higher damping values. These results agree with simple observations made by looking at the time histories that are shown in Fig. 6.

As an example of how well the optimized system matches the experimental results, a comparison between the simulated and measured time histories for Case B is plotted in Fig. 12. The simulated response perfectly matches the measured response.

4. Conclusions

This paper presented a practical crack detection methodology and its verification through experimental case studies. An aluminum bar with different crack configurations was considered in the experimental verification, using a Polytec laser Doppler vibrometer to measure the velocity at a single point on the beam with separate excitations at three different locations. The proposed crack detection methodology consists of two stages.

The number of cracks is identified utilizing the Bayesian model class selection method in the first stage. The updated PDF of the crack locations, extents, the rotational stiffness of the semi-rigid connection, and the damping ratio of first four modes are then identified by the Bayesian model updating method in the second stage.

Very encouraging results were obtained from the experimental case studies. First, the proposed methodology successfully identified the number of cracks in all cases. Second, all identified crack characteristics, such as crack locations and depths, were very close to the true values. One of the outstanding advantages of the proposed methodology is that the uncertainties associated with the identified results can be quantified. As a result, engineers know the confidence level of the crack detection results.

Acknowledgements

The work described in this paper was fully supported by a grant from the Research Grants Council of the Hong Kong Special Administrative Region, China [Projects no. City U 1190/04E].

References

[1] H. Sohn, C.R. Farrar, F.M. Hernez, J.J. Czarnecki, D.D. Shunk, D.W. Stinemates, B.R. Nadler, A review of structural health monitoring literature: 1996–2001, Los Alamos National Laboratory Report, LA-13976-MS, 2004.
[2] D. Liu, H. Gurgenci, M. Veidt, Crack detection in hollow section structures through coupled response measurements, *Journal of Sound and Vibration* 261 (2003) 17–29.
[3] P.F. Rizos, N. Aspragathos, A.D. Dimarogonas, Identification of crack location and magnitude in a cantilever beam from the vibration modes, *Journal of Sound and Vibration* 138 (3) (1990) 381–388.
[4] R.Y. Liang, F.K. Choy, J. Hu, Detection of cracks in beam structures using measurements of natural frequencies, *Journal of the Franklin Institute* 328 (4) (1991) 505–518.
[5] Y. Narkis, Identification of crack location in vibrating simply supported beams, *Journal of Sound and Vibration* 172 (4) (1994) 549–558.
[6] B.P. Nandwana, S.K. Maiti, Modeling of vibration of beam in presence of inclined edge or internal crack for its possible detection based on frequency measurements, *Engineering Fracture Mechanics* 58 (3) (1997) 193–205.
[7] F.G. Tomasel, H.A. Larrondo, Detection of cracks in cantilever beams: experimental set-up using optical techniques and theoretical modeling, *Journal of Sound and Vibration* 228 (5) (1999) 1195–1204.
[8] H.F. Lam, Y.Y. Lee, H.Y. Sun, G.F. Cheng, X. Guo, Application of the spatial wavelet transform and Bayesian approach to the crack detection of a partially obstructed beam, *Thin-Walled Structures* 43 (2005) 1–12.
[9] W.M. Ostachowicz, M. Krawczuk, Analysis of the effect of cracks on the natural frequencies of a cantilever beam, *Journal of Sound and Vibration* 150 (2) (1991) 191–201.
[10] J. Hu, R.Y. Liang, An integrated approach to detection cracks using vibration characteristics, *The Franklin Institute* 330 (5) (1993) 841–853.
[11] S.S. Law, Z.R. Lu, Crack identification in beam from dynamic responses, *Journal of Sound and Vibration* 285 (4–5) (2005) 967–987.
[12] W.F. Chen, N. Kishi, Semirigid steel beam-to-column connections: data base and modeling, *Journal of Structural Engineering* 116 (1) (1989) 105–119.
[13] R.W. Clough, J. Penzien, *Dynamics of Structures*, second ed., McGraw-Hill International Editions, Civil Engineering Series, 2001.
[14] L.S. Katafygiotis, H.F. Lam, C. Papadimitriou, Treatment of unidentifiability in structural model updating, *Advances in Structural Engineering* 3 (1) (2000) 19–39.
[15] H.F. Lam, C.T. Ng, Detection of cracks on a beam by Bayesian model class selection utilizing dynamic data, The Fifth International Conference on Computational Stochastics Mechanics (CSM5), June 21–23, 2006, Rhodes, Greece, 2006.
[16] J.L. Beck, K.V. Yuen, Model selection using response measurement: a Bayesian probabilistic approach, *Journal of Engineering Mechanics, ASCE* 130 (2) (2004) 192–203.
[17] J.L. Beck, L.S. Katafygiotis, Updating models and their uncertainties I: Bayesian statistical framework, *Journal of Engineering Mechanics, ASCE* 124 (4) (1998) 455–461.
[18] L.S. Katafygiotis, J.L. Beck, Updating models and their uncertainties II: model identifiability, *Journal of Engineering Mechanics, ASCE* 124 (4) (1998) 463–467.
[19] C. Papadimitriou, J.L. Beck, L.S. Katafygiotis, Asymptotic expansions for reliability and moments of uncertain systems, *Journal of Engineering Mechanics, ASCE* 123 (12) (1997) 1219–1229.
[20] S.F. Gull, in: J. Skilling (Ed.), *Bayesian Inductive Inference and Maximum Entropy, Maximum Entropy and Bayesian Methods*, Kluwer Academic Publisher, Boston, 1988, pp. 53–74.
[21] H.F. Lam, J.M. Ko, C.W. Wong, Localization of damaged structural connections based on experimental modal and sensitivity analysis, *Journal of Sound and Vibration* 210 (1) (1998) 91–115.
[22] L.S. Katafygiotis, H.F. Lam, Tangential-projection algorithm for manifold representation in unidentifiable model updating problems, *Earthquake Engineering & Structural Dynamics* 31 (4) (2002) 791–812.
[23] L.S. Katafygiotis, C. Papadimitriou, H.F. Lam, A probabilistic approach to structural model updating, *Soil Dynamics and Earthquake Engineering* 17 (7–8) (1998) 495–507.